Journal of Coastal Research	18	4	802–809	West Palm Beach, Florida	Fall 2002

Bar Formation Under Breaking Wave Conditions: A Laboratory Study

Cyril Dulou*, Max Belzons† and Vincent Rey‡

*Département de Géologie et d'Océanographie
UMR 5805 EPOC
Université de Bordeaux I
F-33405 Talence cedex, France
c.dulou@epoc.u-bordeaux.fr

†IUSTI, UMR 6595 du CNRS
Université de Provence
Technople de Château-Gombert
F-13453 Marseille cedex 13, France
belzons@iusti.univ-mrs.fr

‡Laboratoire de Sondages Electromagnétiques de l'Environnement Terrestre
UPRESA-CNRS 6017
Université de Toulon et du Var
BP 132
F-83957 La Garde Cedex, France
rey@lseet.univ-tln.fr

ABSTRACT

DULOU, C.; BELZONS, M., and REY, V., 2002. Bar formation under breaking wave conditions: a laboratory study. *Journal of Coastal Research,* 18(4), 802–809. West Palm Beach (Florida), ISSN 0749-0208.

An analysis of bar formation under breaking waves was carried out in a small-scale wave tank. Although the 1/100 size scale of the tank was unusual for sediment transport study, the results were in agreement with field studies concerning wave breaking criteria and the direction of sand transport. This size permitted accurate simultaneous measurement of the spatial and temporal variations of both the wave height and the bathymetric profile. This study is the extension of a previous one concerned with non-breaking conditions. The role of the nonlinear wave-wave interactions, reinforced under breaking waves, was displayed in the bar formation. Finally, it was suggested that a more realistic modeling of the mean flows distribution in the bottom boundary layer (difference in direction and intensity between the upper and the lower parts) owing to the superposition of the undertow and nonlinearity effects, will improve the modeling of bar formation.

ADDITIONAL INDEX WORDS: *Bar formation, non-breaking waves, breaking waves, nonlinear wave-wave interactions, bedload, suspended load, undertow, wave flume.*

INTRODUCTION

The prediction of shoreline evolution is one of the main challenges in coastal engineering owing to the important social and economic development of the coastal zone. This is particularly relevant for sandy coasts, which may get weakened by any perturbation, one of them, but not the least, may be the sea-level rise induced by the forecast climate changes.

Sand bars are often observed in sandy coastal zones as result of several hydrodynamic forcings (waves, tide, currents) (RUESSINK, 1998). Their sediment budget is related to the evolution of the beach (SCOTT, 1954; SHORT, 1975). A better understanding of sand bar formation would then contribute to better understand and predict shoreline evolution. The field study of bar formation is a very difficult task and is thus often complemented with laboratory experiments (HULSBERGEN, 1974; CHESNUTT, 1975; ROELVINK and STIVE, 1989; ARCILLA *et al.,* 1994; DETTE *et al.,* 1998) and numerical simulations (ZHENG and DEAN, 1997; DEIGAARD *et al.,* 1999; LARSON *et al.,* 1999; BROWDER and DEAN, 2000). Although a considerable effort has been devoted, bar formation is still not well understood and several mechanisms are yet proposed. These mechanisms are reviewed by DEAN *et al.* (1992) and also by VAN RIJN (1998). All these different mechanisms were validated in the field or in the laboratory, and the relevance of each of them depends on the initial wave and bottom conditions (DULOU, 2000). The spatial variation of the wave height, which induces both erosion and acretion zones, is involved in all of them. A simple illustration is the bar formation under a partially-standing and non-breaking regular wave (MEI, 1983; O'HARE and DAVIES, 1990; REY *et al.,* 1995). This non-breaking case allowed to predict the bar formation directly from the wave envelope and so displayed effects of the spatial variation of the wave height on bar formation, which can be present in nature. Thus, the role of nonlinear wave-wave interactions (already present under breaking waves) on bar formation has been studied under non-breaking conditions (DULOU *et al.,* 2000). Under breaking conditions, the simplest proposed mechanism proceeds from the breaking point hypothesis (DYHR-NIELSEN and SØRENSEN, 1970; DEAN *et al.,* 1992): convergence of the Stokes's drift (in the direction of wave advance) and of the undertow (in the opposite direction) at the breaking point. ROELVINK and STIVE (1989) enhanced this hypothesis by including long-wave flow induced by wave group, but bar formation modeling deduced from this mechanism does not show accurate results at the breakpoint or upstream (ZHENG and DEAN, 1997).

This paper presents a small-scale experimental study of bar formation under breaking waves based on an accurate

00172 received 27 December 2000; accepted in revision 18 November 2001.

and simultaneous analysis of both the spatial variations of the wave height and of the bathymetric profile. It aims to correlate spatial wave and bottom modulations, which was displayed under non-breaking wave conditions (DULOU *et al.*, 2000). Three sediment sizes were used allowing the observation of erosional, acretional and intermediate beach states, which in nature are obtained as response to characteristic wave climates (WRIGHT and SHORT, 1984; LARSON and KRAUS, 1993). This work is reported as follow: the experimental facilities are exposed in a first part, the main results obtained under non-breaking conditions are recalled in a second part, the breaking case is presented and discussed in a third part.

EXPERIMENTAL FACILITIES

Both non-breaking and breaking experiments were carried out in a small-scale glass-walled wave flume. The flume is 4.7 m long, 0.39 m wide and the maximum water depth is 0.15 m (Figure 1). A piston-type wavemaker produces a regular wave with a fundamental (or first harmonic) frequency f_0 = 1.5 Hz (with an accuracy of 0.001 Hz). Generally, a spurious free wave having twice the frequency of the fundamental regular wave is observed through a beating in the envelope of the second harmonic (DULOU *et al.*, 1998). This spurious wave is generated by the wavemaker (MADSEN, 1971; HULSBERGEN, 1974; SCHÄFFER, 1996) and has the same frequency as the bound second harmonic of the regular wave, but with a different phase velocity. This spurious wave can be suppressed by placing a sill in front of the wavemaker (HULSBERGEN, 1974; DULOU *et al.*, 2000).

The generated wave, with an initial maximum height of H_0 = 0.02 m, propagates first in a zone of constant water depth, h_0 = 0.08 m, of extend 1.2 m until the toe of a sloping sandy bottom (Figure 1). In the breaking case, a plane sloping ($\beta_{breaking} \sim 0.025$) sandy bed was used, which extend to above the water surface. For the non-breaking case, the slope was more gentle ($\beta_{non\text{-}breaking} \sim 0.01$), and a solid sloping bed of length 0.26 m replaced the sand in the upper part ($h < 0.04$ m). In that case, breaking occurred far downstream of the sand bed (DULOU *et al.*, 2000). In both series of our small-scale experiments, spilling breaking were observed for the initial plane sloping beds. Both breaking mode and location satisfied the criteria of MICHE (1951) and OSTENDORF and MADSEN (1979).

The sediment was an artificial non-cohesive sand formed of glass spheres of density ρ_s = 2.7 10^3 kg.m^{-3}. Three sizes (of diameters 0.08, 0.12 and 0.20 mm) were used for the breaking case and only the 0.08 mm one for the non-breaking case.

The wave height and the bottom location were measured using ultra-sonic sensors: an aerial one for the air-water interface and a submerged one for the water-sediment interface (DULOU, 2000). These sensors allowed measurements of small variations of the bottom or of the free surface with an accuracy of 10^{-4} m. Both sensors were mounted on a carriage which could be translated along the flume by a stepping motor. With this equipment, the envelope of the wave and the bottom profile could be measured easily and precisely.

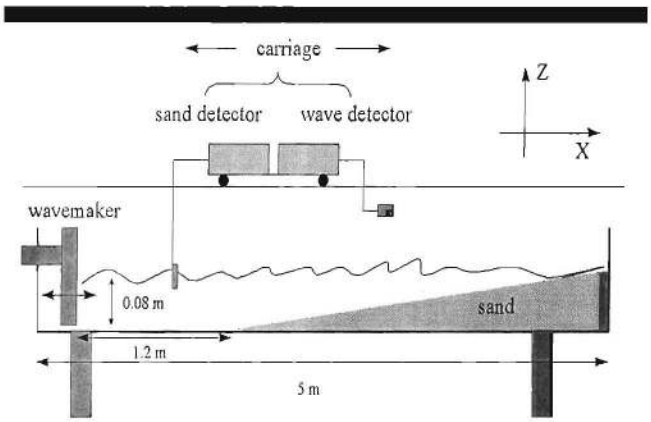

Figure 1. Sketch of the wave flume in the breaking configuration.

EXPERIMENTS WITH NON-BREAKING WAVES

The occurrence of multiple-bar formation, presumably due to non-breaking wave conditions, is observed in nature (SHORT, 1975; DETTE, 1980; MEI, 1983). It was studied extensively in laboratory (SCOTT, 1954; O'HARE and DAVIES, 1990; REY *et al.*, 1995), but these studies were done under constant depth and weakly nonlinear conditions. Additional studies were carried on by DULOU *et al.* (2000) by considering a gently sloping sand bed and also weakly nonlinear waves. We now recall the main results of DULOU *et al.*, (2000), which are needed to better understand laboratory bar formation under breaking waves.

In the previous experiments carried out in our small wave tank (REY *et al.*, 1995; DULOU *et al.*, 2000), it was found that the final bathymetric profile was a replica of the first harmonic spatial modulations. If spatial modulations of half the surface wavelength are explained by a linear approach for partially-standing waves, additional spatial modulations were evidenced in the latest experiments (DULOU *et al.*, 2000), which cannot be explained through linear wave analysis. In particular, the role of nonlinear wave-wave interactions in bar formation was demonstrated for bichromatic waves (monochromatic wave of wavenumber k and frequency f perturbed by a parasitic wave of wavenumber K and frequency $2f$). Indeed, in addition to spatial modulations of wavenumbers close to $2k$, modulations of wavenumbers close to K and $K - 2k$ where also observed in the final bathymetric profile. Such modulations were analytically recovered in the envelope of the fundamental (or first harmonic) wave as demonstrated hereafter. The free surface elevation $\eta(x, t)$ of an incident bichromatic wave is given by:

$$\eta(x, t) = a_1 \cos\left(\omega t - \int k\, dx\right) + A_f \cos\left(\omega t - \int (K - k)\, dx + \varphi_f\right) + a_2 \cos 2\left(\omega t - \int d\, dx\right) + a_f \cos\left(2\omega t - \int K\, dx + \varphi_f\right) \quad (1)$$

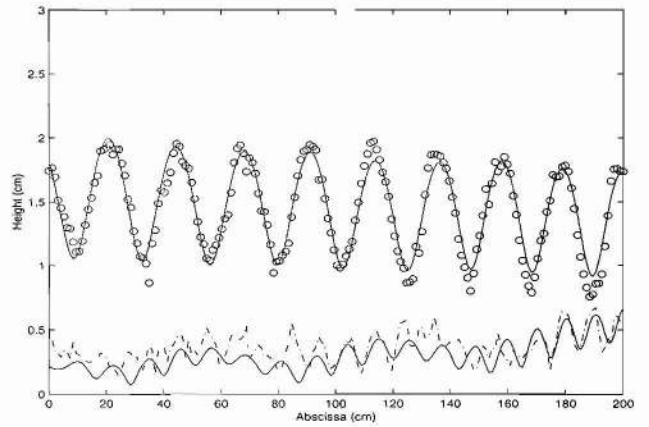

Figure 2. (case 1) Comparison of the envelope of both first and second harmonics for a gently sloping bottom and without any parasitic wave: (——) model, measurements (○) first harmonic, (– – –) second harmonic.

where $\alpha_1 \cos(\omega t - \int k dx)$ and $\alpha_2 \cos 2(\omega t - \int k dx)$ are, respectively the first harmonic and the second harmonic of the regular wave, ω is the wave radian frequency, k the wave number, $\int k dx$ is the phase lag at location x. $\alpha_f \cos(2\omega t - \int K dx + \varphi_f)$ is the parasitic free wave, of wave number K and phase lag φ_f at location $x = 0$. The nonlinear difference interaction between the components of the bichromatic wave is expressed in the term $A_f \cos(\omega t - \int (K - k) dx + \varphi_f)$.

For a partially-standing monochromatic wave perturbed by a spurious wave, the envelope of the first and second harmonics can be calculated by using a form of the Boussinesq equation (MADSEN and SØRENSEN, 1993; DULOU, 2000). Writting $\eta(x, t) = A^{(\omega)}(x)\cos(\omega t) + A^{(2\omega)}(x)\cos(2\omega t) + \ldots$, the envelope of the first and second harmonic wave are then given at leading orders by:

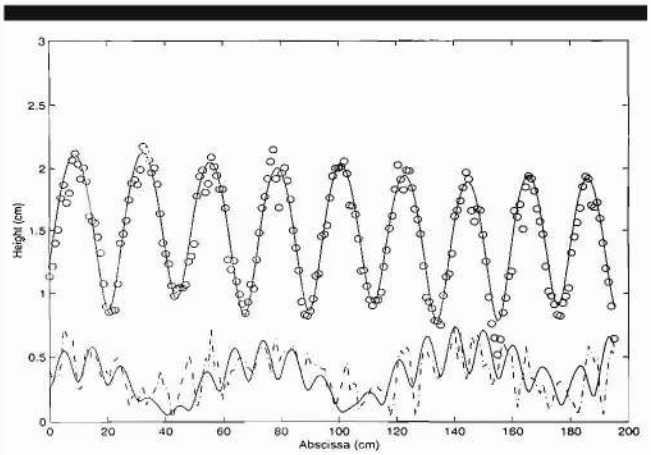

Figure 3. (case 2) Comparison of the envelope of both first and second harmonics for a gently sloping bottom and without any parasitic wave: (——) model, measurements (○) first harmonic, (– – –) second harmonic.

Table 1. *Parameters introduced in the model after a least square method fit.*

Parameters	Case 1	Case 2
a (cm)	0.76	0.77
a_f (cm)	0.04	0.12
ϕ_f (rad)	5.95	1.25
R_b	0.31	0.40
ϕ (rad)	0.69	3.80
R_2	0.3	0.24
ϕ_2 (rad)	3.3	1.54

$$A^{(\omega)}(x) = a_1\Bigg[1 + R_b^2 + 2R_b\cos\Big(2\int k\,dx + \varphi\Big) + \frac{2A_f}{a_1}\Bigg(2R_b\cos\varphi_f\cos\Big(\int K\,dx + \varphi\Big) + \cos\Big(\int (K - 2k)\,dx - \varphi_f\Big) + R_b^2\cos\Big(\int (K - 2k)\,dx + \varphi_f\Big)\Bigg)\Bigg]^{1/2} + O\left(\frac{a_1 a_f^2}{h^2}\right) \quad \text{and} \tag{2}$$

$$A^{(2\omega)}(x) = \Bigg[a_f^2\Big(1 + R_2^2 + 2R_2\cos\Big(2\int K\,dx + \varphi_2\Big)\Big) + a_2^2\Big(1 + R_b^2 + 2R_b\cos\Big(4\int k\,dx + \varphi\Big)\Big) + a_f a_2\Bigg(\cos\Big(\int (K - 2k)\,dx - \varphi_f\Big) + R_b\cos\Big(\int (K + 2k)\,dx \quad \varphi_f + \varphi\Big) + R_2\cos\Big(\int (K + 2k)\,dx + \varphi_f + \varphi_2\Big) + R_b R_2\cos \times \Big(\int (K - 2k)\,dx + \varphi_f + \varphi_2 - \varphi\Big)\Bigg)\Bigg]^{1/2} \tag{3}$$

where $O(A_f/a_1) = a_f/h$, R_b is the modulus of the beach reflection coefficient and φ is the phase lag between incident and reflected waves. R_2 is the reflection coefficient of the parasitic wave and φ_2 its phase lag.

Eq. 2 shows that the envelope of the first harmonic is a combination of cosine components, of respective wavenumbers close to $2k$, K and $K - 2k$, depending on the reflection. Figures 2 and 3 show the good agreement between the model and measurements of the envelope of the first harmonic, respectively without (case 1) and with (case 2) the presence of a parasitic wave. The different parameters were obtained by using a least square method and the results are presented in Table 1.

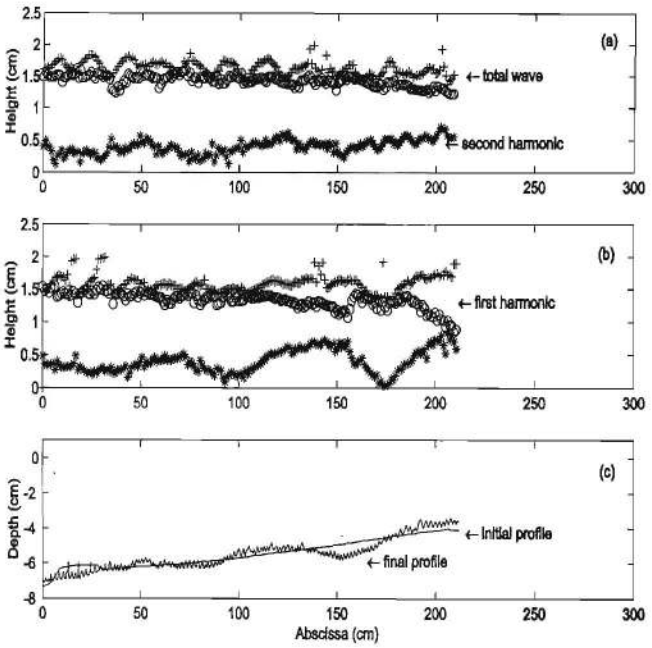

Figure 4. Envelope of the initial wave (a), final (b) and bathymetric profile (c) after 2660 min of wave action under non-breaking conditions (H_0 = 1.7 cm and $R_b < 0.05$, D_1 = 0.08 mm).

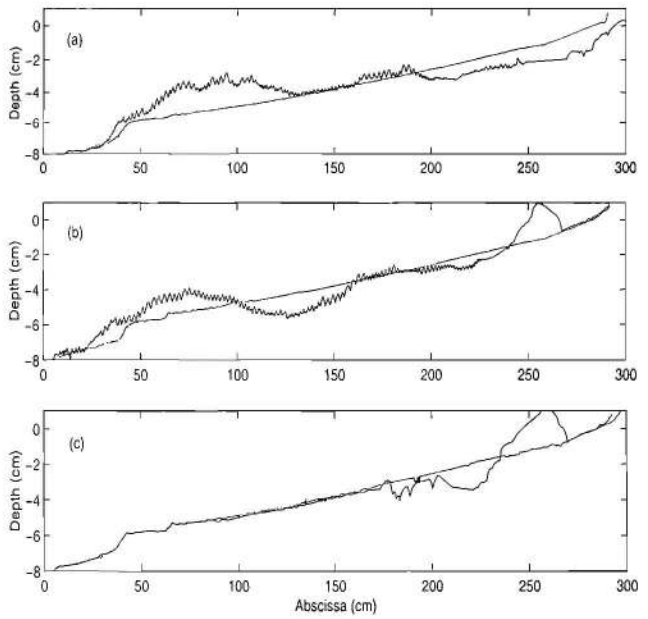

Figure 5. Final bathymetric profiles under breaking conditions for D_1 = 0.08 mm and ψ_{D_1} = 34.3 (suspended load) (a), D_2 = 0.12 mm and ψ_{D_2} = 22.9 (intermediate) (b) and D_3 = 0.20 mm and ψ_{D_3} = 13.7 (bedload) (c) (H_0 = 1.9 cm, H_b = 2.5 cm and h_b = 2.9 cm).

The comparison of both model and experimental envelope of the second harmonic is less accurate because only one spurious wave was taken into account. More accurate results would need to consider also parasitic waves of higher frequencies or spatial varying free wave amplitudes.

Eq. 2 shows that if the reflection is close to zero, that is, if wave conditions are close to the natural case of a gentle beach slope, only one spatial modulation is present in the envelope of the first harmonic: the biggest one, $2\pi/(K - 2k)$, which represents the nonlinear interaction between both free waves. Effectively, this theoretical result is confirmed by the Figure 4 which presents the final equilibrium profile modulated with the same length than the one of the interaction which corresponds to the spatial wavelength $2\pi/(K - 2k)$ (which is 8.77 m^{-1}, K = 37.89 m^{-1} and k = 14.56 m^{-1} for the mean water depth h = 0.05 m, corresponding to the wavelength 0.7164 m). This last result displayed the role of the nonlinear wave-wave interactions in sediment transport and finally in bar formation.

As these nonlinear interactions increase with the decreasing water depth and are particularly important in the shoaling and breaking zones, we then studied bar formation under breaking wave conditions.

EXPERIMENTS WITH BREAKING WAVES

We remind that for the breaking case, a gently sloping sand bed ($\beta \simeq 0.025$) is located from h_0 = 0.08 m of water depth to the shoreline. So, the breaking occurs above the sediment layer. In these experiments, the incoming wave was monochromatic by suppressing the parasitic wave.

The three grain sizes (of respective mean diameter D_1 = 0.08 mm, D_2 = 0.12 mm, D_3 = 0.20 mm) were used to study the effect of transport modes on bar formation. The observation showed a lot of suspension with the finest sediment (D_1 = 0.08 mm) and no suspension for the biggest one (D_3 = 0.20 mm). For the intermediate one D_2 = 0.12 mm), suspension was only observed around the breakpoint. The final profiles obtained under the same wave conditions (incident wave height H_0 = 1.9 cm, breaking wave height H_b = 2.5 cm and water depth at breaking h_b = 2.9 cm) are presented in the Figure 5. The breakpoint was located at x_b = 205 cm. In term of mobility number (NIELSEN, 1992), $\psi = (u_0^2)/(s - 1)gD_{50})$ (where u_0 is maximum velocity just above the boundary layer, $s = \rho_s/\rho$ is relative density, g is gravity constant and D_{50} is mean grain diameter of the sediment) varied from 34.3 to 13.7 for respectively the finest to the biggest sediment. The nondimensional parameter $\Omega = H_b/(\omega_s T)$, where ω_s is sediment fall velocity and T is wave period, is often used for classifying bar and berm profiles (WRIGHT and SHORT, 1984): bar formation (erosion) if $\Omega > 6$, berm formation (acretion) if $\Omega < 1$ and intermediate state (bar and berm formation) if $1 < \Omega < 6$.

Figure 5 shows that the direction of sand propagation depends on the nature of transport under breaking wave conditions. In suspension-dominated case (Ω_{D_1} = 6.3), a bar is formed upstream from the breaking point whereas a bar is formed after the breaking point in the bedload-dominated case (Ω_{D_3} = 1). We found an intermediate case (Figure 5b), where a bar and a berm were formed (Ω_{D_2} = 2.8).

This observation is in accordance with the field observations where a berm is formed by low wave amplitude and an

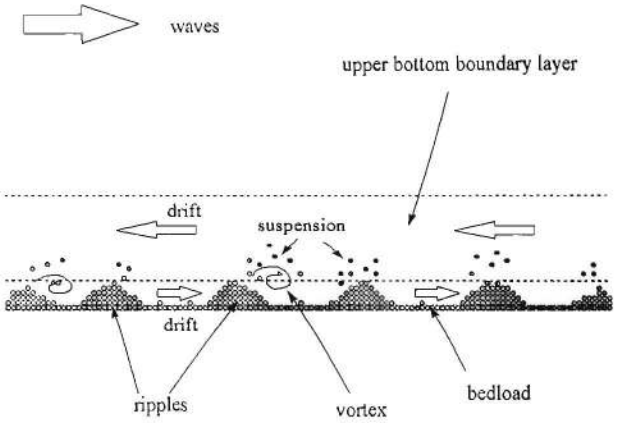

Figure 6. Vertical repartition of mean flows in the bottom boundary layer far upstream from the breaking point.

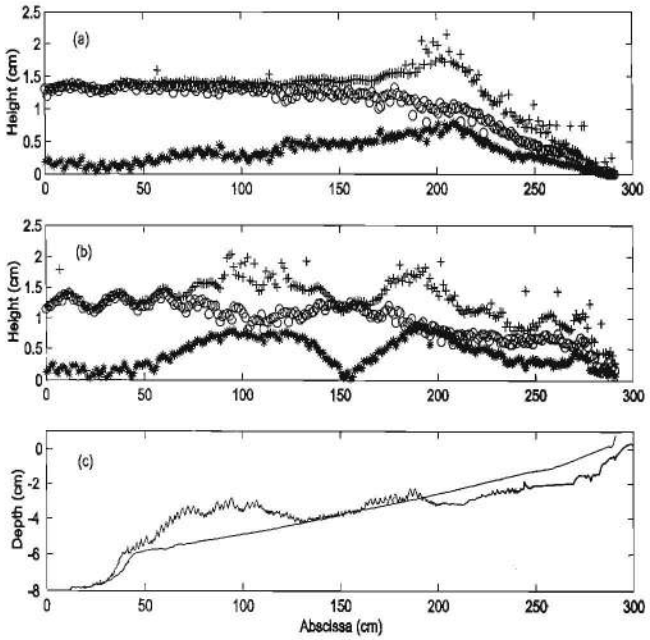

Figure 7. Envelope of the initial wave (a), and final (b) and bathymetric profile (c) after 4660 min of wave action under breaking conditions (H_0 = 1.9 cm, D_1 = 0.08 mm).

offshore bar is formed by storm since according to the non-dimensional form of Ω, an increase of the wave energy at a fixed sediment size corresponds to a decrease of the sediment size at fixed wave energy. It is also in accordance with the classification by synthesis of many field data of WRIGHT and SHORT (1984).

Moreover, DAVIES and VILLARET (1999) have calculated the Eulerian drift induced by asymmetrical progressive and non-breaking waves in the bottom boundary layer above rippled and very rough beds. They found that the near-bed flow, bedload precursor, was in the direction of the wave advance, and the flow at the edge of the boundary layer was in the opposite direction. Figure 6 is an illustration of these results. Our small-scale observations seem to confirm these theoretical results.

The suspension-dominated case (D_1 = 0.08 mm) is now considered and compared with the non-breaking and low reflection experiments. Figure 7 presents both initial and final envelopes and the final bathymetric profile. In the initial wave envelope (Figure 7a), the height of the first harmonic of the wave starts to decrease from x = 120 cm, whereas the height of the second harmonic increases until the breakpoint (x_b = 205 cm), and then decreases, in the same way as the first harmonic. The final wave envelope (Figure 7b) looks like the non-breaking one (Figure 4b): upstream from the breakpoint, there is a beating in the envelope of the second harmonic and a bar is observed in that zone, as in the bichromatic non-breaking case. In both cases the configurations of the envelope-bar system over the extend of the beating are very similar.

Although, no parasitic wave was initially present in the breaking case (no beating appears initially in the envelope of the second harmonic), whereas it was present in the non-breaking case, the final envelope of the second harmonic reveals the appearance of an additional free harmonic through the beating observed from x = 50 cm to x = 150 cm.

To resume, non-breaking experiments showed that, in the case of low reflection and in presence of a parasitic wave, a beating was observed in both the initial and final envelope of the second harmonic. DULOU *et al.* (2000) have demonstrated that the parasitic wave, due to the wavemaker, perturbed the first harmonic envelope which drove bar formation. The bar was then of the same length as the beating. In the breaking experiment, both a beating and a bar of the same length scale were observed in the final measurements although no beating was present in the initial envelope. So, the questions are: is it the same mechanism of bar formation as in the non-breaking case? What is the origin of the beating in the final envelope?

From the above described experimental results, the strongly nonlinear part of the wave just before the breaking point (decrease of the first harmonic amplitude) was suspected to play an important role in bar formation. In order to check this hypothesis, the initial bottom was modified to preserve highly nonlinear wave conditions but in a zone located far away from breaking and thus poorly affected by the undertow. This was obtained by placing an horizontal sandy zone (of 0.8 m long) prolonged downstream with an inclined solid plate where the breaking occurred.

Figure 8 shows the wave envelope and both the initial profile and the profile after 60 min. The wave is very nonlinear above the horizontal part (both first and second harmonics have a similar amplitude) and the breaking occurs only when the bathymetry is again decreasing, that is on the solid plate of which slope is about 0.10. After 60 min, small length scale bars are formed with a length of half the local wavelength of the wave, according to Bragg conditions (DULOU *et al.*, 2000). These bars could contribute to the increase of the reflection (MEI, 1983; O'HARE and DAVIES, 1990; DULOU *et al.*, 2000). A beating is observed in the envelope of the second harmonic

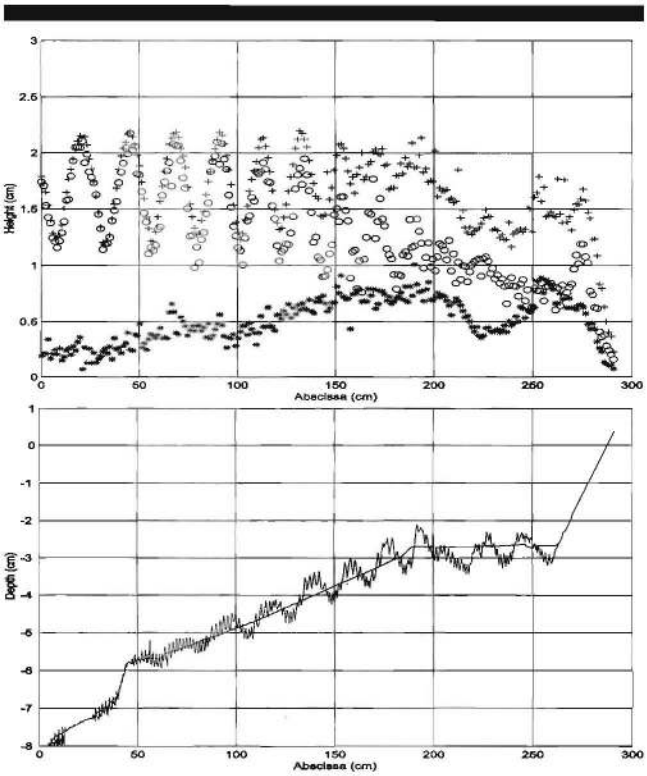

Figure 8. (a) Envelope of (+) the total wave and of (○) first and (*) second harmonics at 60 min, above (b) the initial bathymetric profile (– – –) and at 60 min (——) (H_0 = 1.6 cm and D_1 = 80 μm.

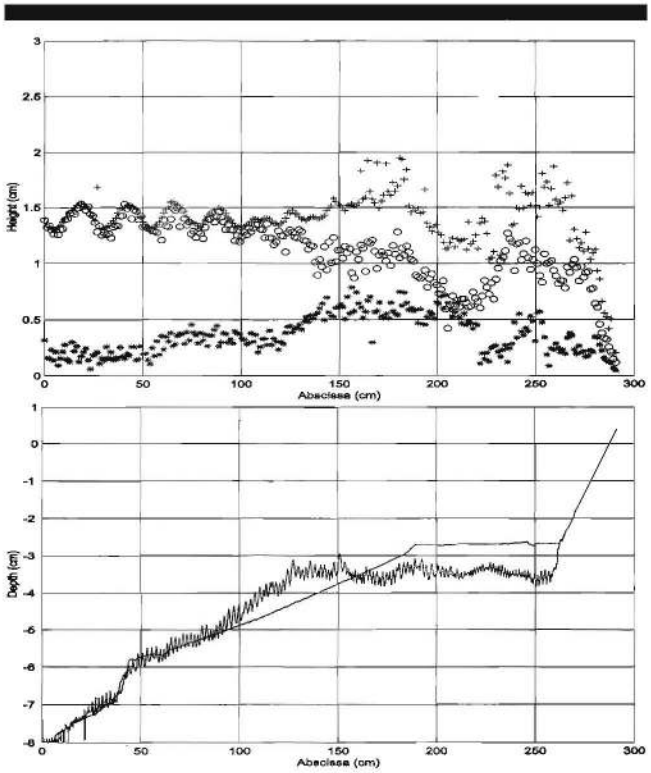

Figure 9. (a) Envelope of (+) the total wave and of (○) first and (*) second harmonics at 1320 min, above (b) the initial bathymetric profile (– – –) and at 1320 min (——) (H_0 = 1.6 cm and D_1 = 80 μm.

from x = 100 cm to x = 220 cm suggesting a local production of free harmonics which interact with the bound ones. In the non-breaking case this production was external and forced by the wavemaker, whereas in this case the production of free harmonic is natural and locally induced by bathymetric changes. Indeed, several experimental (BATTJES and BEJI, 1992; ARCILLA *et al.*, 1994) and numerical studies (MADSEN *et al.*, 1997; GRILLI and HORRILLO, 1999) have shown the release of bound harmonics in the deshoaling zone.

The final envelope of the second harmonic (Figure 9a) shows the same length scale beating from x = 120 cm to x = 220 cm. In the final bathymetric profile (Figure 9b), small-scale bars have disappeared and only a larger bar is present from x = 80 cm to x = 170 cm. The bar length is then of the same order as the beating length, like in the standard breaking case. The sediment was transported in the offshore direction.

Finally, the bar was formed as in the standard breaking case, under the same nonlinearity conditions, but with a strongly diminished action of the undertow, which means that the sediment was transported in the seaward direction by another mechanism than undertow. Then, this offshore mean current was only due to the nonlinearity, in total agreement with the results of DAVIES and VILLARET (1999) in the suspension-dominated case. The volume of the bar was also smaller than in the standard breaking case. It is certainly due to the larger sandy surf zone and to the superposition of the undertow and of the offshore drift due to the nonlinearities over a rippled bed in the standard case. This superposition could also explain the large value of the mean flow in the seaward direction measured far upstream from the breakpoint (TING and KIRBY, 1994) whereas some experimental or theoretical considerations concluded that the undertow stops at the breakpoint (LONGUET-HIGGINS, 1983). Figure 10 resumes the mean flows considerations around the breaking point.

CONCLUSION

The density and the accuracy of the measurements in a small-scale wave flume allowed observations of the spatial and temporal evolution of bar formation resulting from the wave-sand bed interaction under breaking wave conditions. Whereas the hydrodynamic scale of this study is very small (≅ 1/100), bar and berm formations seem to be in accordance with field studies. This study has shown the dependency of bar formation on the mode of sediment transport, which means that the mean flow in the bottom boundary layer is stratified: there is a difference in the direction of the mean flow between the upper part of the boundary, where suspension is located, and the near bed mean flow where bedload dominates. This reversal of flow direction was also present in the surf zone, even under the action of the undertow.

The second important result of this study concerns the suspension-dominated case and the role of both the nonlinear

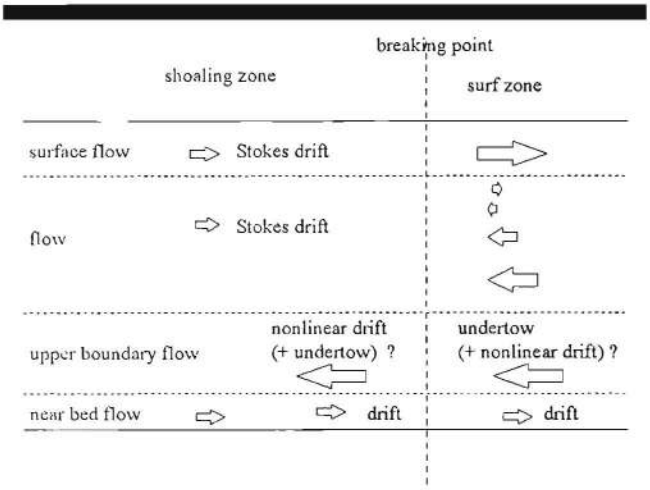

Figure 10. Vertical repartition of mean flows around the breaking point.

wave-wave interactions and the undertow in bar formation. Indeed, by increasing complexity of the experimental conditions (non-breaking waves → breaking waves), we observed that the formation of a long bar is associated with a beating in the wave envelope of the second harmonic, under both non-breaking and breaking wave conditions. The last experiment has demonstrated that a bar is formed even under lowered action of the undertow, thanks to the nonlinearities that control the mean flows. This result could explain bar formation far from the breakpoint or the offshore migration of the bars. In any case, it demonstrated that spatial modulations in the wave envelope may be at the origin of bottom evolution, which cannot be predicted by linear wave analysis (contrary to modulations due to partially-standing waves).

The breaking point mechanism of bar formation could be improved by considering the near bed flow, which can be different in direction, and an additional flow in the same direction as the undertow. Nevertheless, these mean flows are related to the position of the breakpoint which means that this position is indeed an important parameter in bar formation. The next stage of this study would be then the issue of the influence of the breakpoint location on bar formation under action of bichromatic waves or irregular wave group.

ACKNOWLEDGMENTS

Financial support by the French scientific program PNEC (Programme National d'Environnement Côtier) is acknowledged. The authors are grateful to the referees of this paper: they can find here our gratitude for their critical and constructive comments.

LITERATURE CITED

ARCILLA, A.S.; ROELVINK, J.A.; O'CONNOR, B.A.; RENIERS, A., and JIMENES, J.A., 1994. The delta flume '93 experiment. *Proceedings of the Coastal Dynamics Conference* (Barcelona, Spain), pp. 488–502.

BATTJES, J.A. and BEJI, S., 1992. Breaking waves propagating over a shoal. *Proceedings of the 23rd Coastal Engineering Conference* (ASCE), pp. 42–50.

BROWDER, A.E. and DEAN, R.G., 2000. Monitoring and comparison to predictive models of the Perdido Key beach nourishment project, Florida, USA. *Coastal Engineering*, 39, 173–191.

CHESNUTT, C.B., 1975. Laboratory effects in coastal movable-bed models. *Proceedings of the 2nd Symp. Model. Tech.* (ASCE), 2, pp. 945–961.

DAVIES, A.G. and VILLARET, C., 1999. Eulerian drift induced by progressive waves above rippled and very rough beds. *Journal of Geophysical Research*, 104, 1465–1488.

DEAN, R.G.; SRINIVAS, R., and PARCHURE, T.M., 1992. Longshore bar generation mechanisms. *Proceedings of the 23rd Coastal Engineering Conference* (ASCE), 1, pp. 2001–2014.

DEIGAARD, R.; JAKOBSEN, J.B., and FREDSØE, J., 1999. Net sediment transport under wave groups and bound long waves. *Journal of Geophysical Research*, 104, 13559–13575.

DETTE, H.H., 1980. Migration of longshore bars. *Proceedings of the 17th Coastal Engineering Conference*, 1, pp. 1476–1492.

DETTE, H.H.; PETERS, K., and NEWE, J., 1998. Large wave flume experiments '96/97, Report No. 825, MAST III-SAFE Project.

DHYR-NIELSEN, M. and SØRENSEN, T., 1970. Some sand transport phenomena on coasts with bars. *Proceedings of the 12th Coastal Engineering Conference* (ASCE), pp. 855–866.

DULOU, C.; REY, V., and BELZONS, M., 1998. Bar formation on a sloping erodible bed: A laboratory study. *Proceedings of the 13th Australasian Fluid Mechanics Conference* (Melbourne, AFMC), 2, pp. 815–818.

DULOU, C.; BELZONS, M., and REY, V., 2000. Laboratory study of wave-bottom interaction in the bar formation on an erodible sloping bed. *Journal of Geophysical Research*, 105, 19745–19762.

DULOU, C., 2000. Interactions houle-sédiments: application à la formation des barres littorales, thèse, Université de Provence, 185p.

GRILLI, S.T. and HORRILLO, J., 1999. Shoaling of periodic waves over barred-beaches in a fully nonlinear numerical wave tank. *International Journal of Offshore and Polar Engineering*, 9, 257–263.

HULSBERGEN, C.H., 1974. Origin, effect and suppression of secondary waves. *Proceedings of the 14th Coastal Engineering Conference*, pp. 392–411.

LARSON, M. and KRAUS, N.C., 1993. Dynamics of longshore bars. *Proceedings of the 23rd International Coastal Engineering Conference* (ASCE).

LARSON, M.; KRAUS, N.C., and WISE, R.A., 1999. Equilibrium beach profiles under breaking and non-breaking waves. *Coastal Engineering*, 36, 59–85.

LONGUET-HIGGINS, M.S., 1983. Wave set-up, percolation and undertow in the surf zone. *Proceedings of the Royal Society of London*, A 390, 283–291.

MADSEN, O.S., 1971. On the generation of long waves. *Journal of Geophysical Research*, 76, 8672–8683.

MADSEN, P.A. and SØRENSEN, O.R., 1993. Bound waves and triads interactions in shallow water. *Ocean Engineering*, 20, 359–388.

MADSEN, P.A.; SØRENSEN, O.R., and SCHÄFFER, H.A., 1997. Surf zone dynamics simulated by a Boussinesq type model. part 1. Model description and cross-shore motion of regular waves. *Coastal Engineering*, 32, 255–287.

MEI, C.C., 1983. *The applied dynamics of ocean surface waves.* Wiley-Interscience.

MICHE, R., 1951. Le pouvoir réfléchissant des ouvrages maritimes exposés à l'action de la houlse, *Annales des Ponts et Chaussées, 121ème* annexe, pp. 285–319.

NIELSEN, P., 1992. *Coastal Bottom Boundary Layers and Sediment Transport.* World Scientific.

O'HARE, T.J. and DAVIES, A.G., 1990. A laboratory study of sand bar evolution. *Journal of Coastal Research*, 6, 531–544.

OSTENDORF, D.W. and MADSEN, O.S., 1979. Analysis of longshore currents and associated sediment transport in the surf zone. *MIT rep., Sea Grant.*

REY, V.; DAVIES, A.G., and BELZONS, M., 1995. On the formation of bars by the action of waves on an erodible bed: a laboratory study. *Journal of Coastal Research*, 11, 1180–1194.

ROELVINK, J.A. and STIVE, M.J.F., 1989. Bar-generating cross-shore flow mechanisms on a beach. *Journal of Geophysical Research*, 94, 4785–4800.

RUESSINK, B.G., 1998. Infragravity waves in a dissipative multiple bar systems, Thesis, Utrecht University.
SCHÄFFER, H.A., 1996. Second-order wavemaker theory for irregular waves. *Ocean Engineering,* 23, 47–88.
SCOTT, T., 1954. *Sand movement by waves,* Technical Report, No. 48, Beach Erosion Board, U.S. Army Corps of Engineers.
SHORT, A.D., 1976. Offshore bars along the Alaskan Arctic coast. *Journal of Geology,* 83, 209–221.
TING, F.C.K. and KIRBY, J.T., 1994. Observation of undertow and turbulence in a laboratory surf zone. *Coastal Engineering,* 24, 51–80.
VAN RIJN, L.C., 1998. *Principles of coastal morphology,* Aqua Publications, Amsterdam.
WRIGHT, L.D. and SHORT, A.D., 1984. Morphodynamic variability of surf zones and beaches: a synthesis. *Marine Geology,* 56, 93–118.
ZHENG, J. and DEAN, R.G., 1997. Numerical models and intercomparisons of beach profile evolution. *Coastal Engineering,* 30, 169–201.